Noda *et al. ROBOMECH Journal* (2023) 10:25
https://doi.org/10.1186/s40648-023-00264-w

ROBOMECH Journal

RESEARCH ARTICLE

Open Access

Switching backdrivability of a planetary gear by vibration: design parameter setting and excited force estimation

Satsuya Noda[1*], Ryo Igari[1], Kensuke Endo[1], Kazushi Yamanobe[1] and Toshio Takayama[2]

Abstract

Switching backdrivability according to use status is important to attain energy-saving and compliance in co-worker robots. Authors have proposed switching backdrivability by exciting gear surface, eliminating the need for sensors while switching. We have confirmed that exciting 2K-H planetary gear can switch its backdrivability. To systematically design the switching backdrivable 2K-H planetary gear, this study reveals less back-drive condition and the required torque for a vibrator. In the less-backdrivable condition, the tooth number difference between the fixed and output gears is dominant. Furthermore, the required torque for the vibrator increases as the load of the output shaft and the vibration frequency increase. The experimental results of the less-backdrivable condition and the required torque for the vibrator are almost entirely consistent with simulation result of the mechanical model

Keywords Planetary gear, Backdrivability, Vibration, Eccentric cam

Introduction

Reducers without backdrive are used in industrial robots to reduce energy consumption of the manipulator while maintaining its posture. Alternatively, to manually drive a manipulator during an emergency stop, reducers for co-worker robots (e.g., wearable robots and exoskeleton robots) need compliance control. Switching compliance according to the use status is significant to attain energy-saving and compliance for robots. General soft robots [1–4] can easily attain compliant motion but have difficulty in reducing compliance compared with general industrial robots. To switch compliance of general industrial robots, the use of backdrivable reducers with lock mechanisms (e.g., clutch and brake) is significant, but requires complicated control. Alternatively, controlling the backdrivability of no-backdriven reducers with sensors [5] is still complex, resulting in low reliability. Thus, switching backdrivablity without complex control for no-backdriven reducers is required to enhance reliability.

Because backdrivability depends on the friction caused by the reducer gears, our studies focused on reducing friction by vibration. Researchers have developed devices which reduced friction by vibration [6–8]; however, these studies do not focus on backdrivability of reducers. Our research group has proposed switching backdrivability by exciting the gear surface [9], eliminating the need for sensors. Apart from the clutch mechanism, the proposed method does not shut down the power transmission path, reducing the risks of secondary disaster. Takayama et al. examined the switching backdrivability in worm gears [9–11].

However, the skew output shaft of a worm gear limits its application, and the vibrator slight actuation to the output shaft could cause secondary disaster. To apply these methods to general robots more safely, the types of applicable reducers should be increased. To gain a

*Correspondence:
Satsuya Noda
snoda@fukushima-nct.ac.jp
[1] Department of Mechanical System Engineering, National Institute of Technology, Fukushima College, 30 Tairakamiarakawa-aza-Nagao, Iwaki, Fukushima 970-8034, Japan
[2] Department of Mechanical Engineering, Tokyo Institute of Technology, 2-12-1, Ookayama, Meguro-ku, Tokyo 152-8552, Japan

reduction ratio of −1/100 other than the worm gear, planetary gears are generally used for industrial robots. Thus, this study focuses on planetary gears for less-backdriven reducers for switching backdrivability. There exists a less-likely-backdriven planetary gear using spur gear [12]. In addition, we had confirmed that exciting 2K-H planetary gear [13, 14] can switch its backdrivability [15, 16]. However, because the design parameters of the proposed system are determined by trial and error, the planetary gear switching backdrivability phenomenon is not obvious.

To systematically design the switching backdrivable 2K-H planetary gear, this study reveals less back-drive condition and the required torque for a vibrator. We first discuss the less-likely-backdriven structure of the 2K-H planetary gear [13] and then estimates the excitation force for switching backdrivability to select the vibrator. The dynamic model enables calculation of the excitation force for switching backdrivability. This study does not focus on reducing the vibrator's energy consumption because it is used only in emergencies.

The remaining paper is organized as follows: "Modeling of the vibrating planetary gear" section discusses the mechanical analysis of the less-backdriven structure and the excitation force; "Simulation and Experiments" section verifies the effectiveness of the proposed mechanical model; "Discussion" section describes the limitations of the proposed method and "Conclusion" section concludes this study.

Modeling of the vibrating planetary gear

Figure 1 shows the concept of the switching system for a planetary gear. The carrier is excited in the axial direction to reduce friction between gear surfaces. This study uses standard gears and coulomb friction model. Let G_i be the ith gear as shown in Fig. 1, and Z_i be the tooth number of gear G_i. The reduction ratio ρ is given by

$$\frac{1}{\rho} = 1 - \frac{Z_1}{Z_2}\frac{Z_3}{Z_4}, \tag{1}$$

where the sign of ρ denotes the rotational direction: if the sign is positive, the rotational direction of the motor and output side is the same. Figure 2 shows a front view of the proposed planetary gear and an expanded view of the tooth meshing of the proposed planetary gear. The spur gear parameters include the following:

α: pressure angle ($= 20°$)

n: tooth number difference between G_1 and G_4 ($n = |Z_1 - Z_4|$)

F_{ijn}: normal force to to G_i and G_j surface

F_{ijt}: tangential force to G_i and G_j surface

F_{rot}: force acting on G_2 and G_3 axis (see Fig. 2)

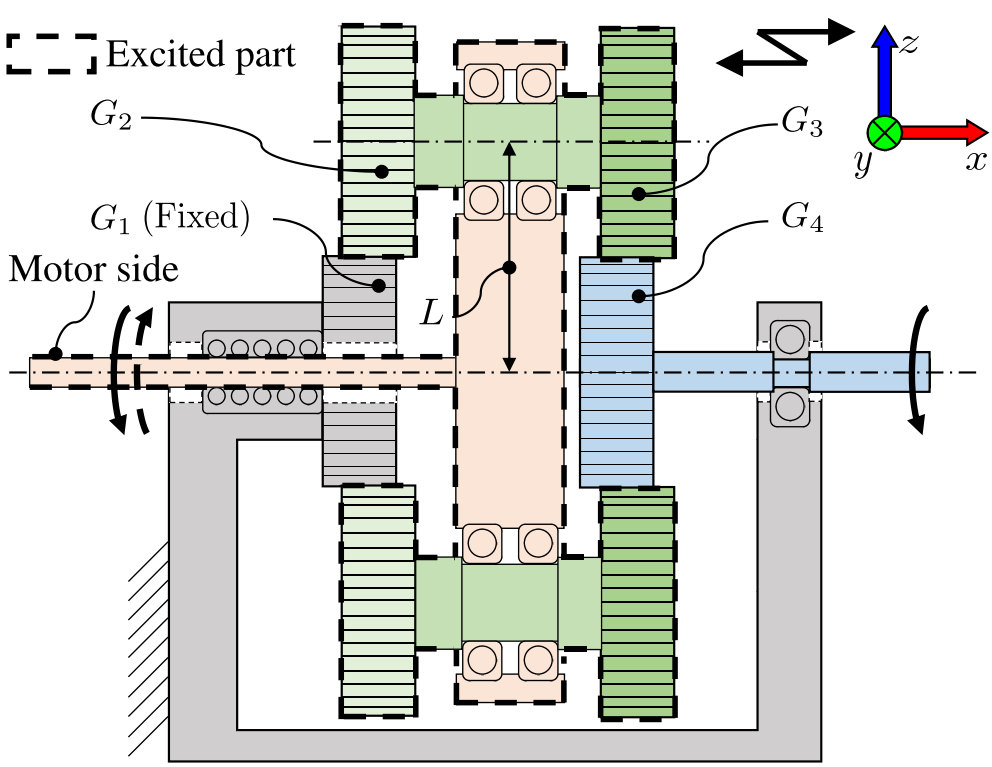

Fig. 1 Idea of switching backdrivability in 2K-H planetary gear. The carrier is excited in the axial direction

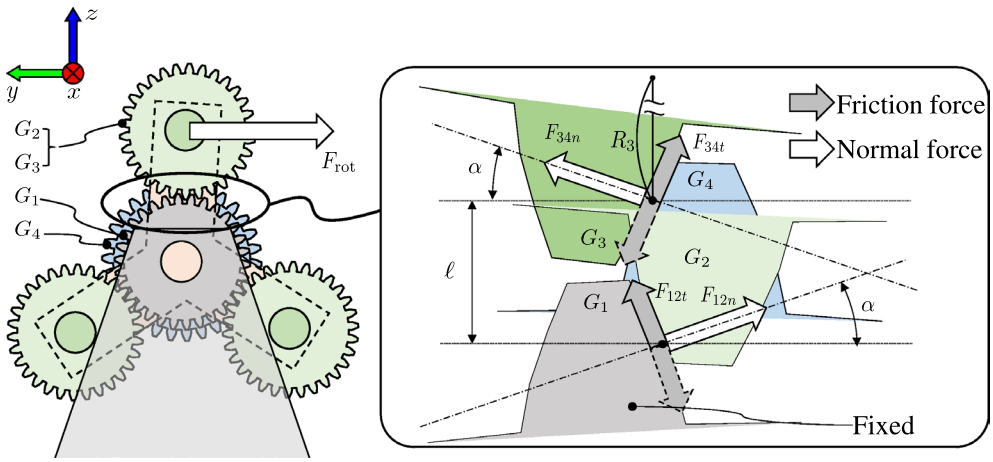

Fig. 2 Force acting on the carrier and gears

m_{ij}: module of G_i and G_j
R_i: radius of the pitch circle of G_i
ℓ: difference between R_1 and $R_4 (= R_1 - R_4)$
b_{sign}: sign of ℓ $(= \mathrm{sgn}(\ell))$
M_1: mass of the input shaft and carrier
I_1: inertia moment of the input shaft and carrier
M_{23}: mass of G_2 and G_3
I_{23}: inertia moment of G_2 and G_3
I_4: inertia moment of the output shaft
L: radius of the carrier
ω_t: angular velocity of G_4
ω_n: angular velocity of vibration
τ_{rot}: torque acting on G_4 axis
ε_i: approach or recess contact ration of G_i and is calculated as [17]

$$\varepsilon_i = \frac{Z_i}{2\pi}\left(\frac{\sqrt{(Z_i+2)^2 - Z_i^2\cos^2\alpha}}{Z_i\cos\alpha} - \tan\alpha\right). \tag{2}$$

μ: coefficient of friction
μ_{ij}: coefficient of friction between G_i and G_j (detail is described in the later section; static coefficient of friction = 0.271, dynamic coefficient of friction = 0.174) Because the material and manufacturing of G_1 to G_4 is identical, this study assumes $\mu = \mu_{12} = \mu_{34}$.
μ_d: dynamic coefficient of friction
μ_s: static coefficient of friction

Less-likely-backdrive condition of the proposed planetary gear

Although backdrivability depends on real engagement situations, this paper discusses backdrivability tendency based the average efficiency engagement situations. Therefore, this paper defines less-likely-backdrive condition as no-backdrive tendency based on the average efficiency engagement situations. This section describes the less-likely-backdrive condition of the proposed planetary. Let Λ be the constant defined by

$$\Lambda = \frac{\pi\left(2 - \sum_{i=1}^{4}\varepsilon_i + \sum_{i=1}^{4}\varepsilon_i^2\right)}{n}. \tag{3}$$

Because the planetary gear is static in this state, this section uses static analysis. From motion equation analysis as described in "Appendix" section, the proposed mechanism is less likely to backdrive when

$$\mu\Lambda > 1. \tag{4}$$

Herein, we consider the value of Λ. Let k' be the design parameter of Z_2 defined by

$$k' = \frac{Z_2}{Z_1}. \tag{5}$$

Fig. 3 shows the relationship between Λ and Z_1. Λ increases as Z_1, k', and $\frac{1}{n}$ increase. However, compared with Z_1 and k', n causes more changes in Λ, making it the dominant parameter. Hence, to generate less-likely-backdriven condition in the 2K-H planetary gear, the adjustment of n is significant.

Behavior of the output shaft during backdriven state

This section states behavior of the output shaft during backdriven state using the dynamic model. The motion equation of the proposed planetary gear is calculated by

$$\widehat{I}\frac{d\omega_t}{dt} + \tau_{\mathrm{rot}}\frac{\mu_d\Lambda|\omega_t|}{\sqrt{\omega_t^2 + \lambda^2\omega_n^2}} = \tau_{\mathrm{rot}}, \tag{6}$$

where $\widehat{I}$ denote the equivalent moment of inertia given by

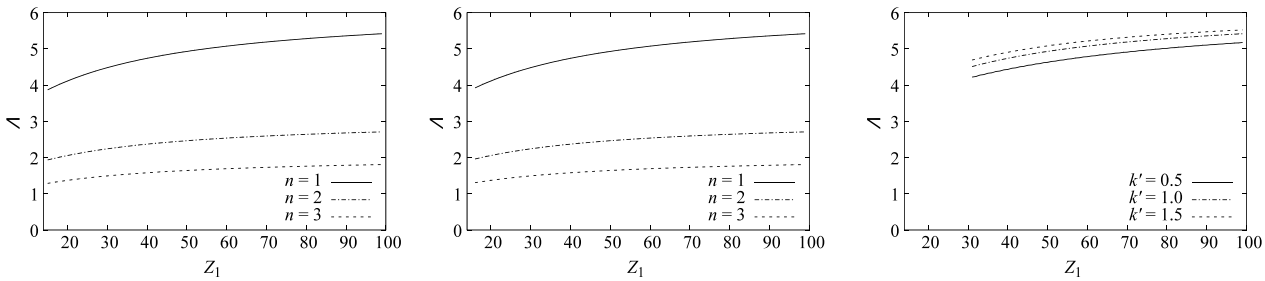

(a) $k' = 1,\ Z_1 > Z_4$. (b) $k' = 1,\ Z_1 < Z_4$. (c) $n = 1,\ Z_1 > Z_4$.

Fig. 3 Λ versus Z_1

$$\widehat{I} = I_1\rho^2 + M_{23}(R_1+R_2)^2\rho^2 + I_{23}\left(1+\frac{Z_1}{Z_2}\right)^2\rho^2 + I_4. \tag{7}$$

Detail of the derivation is described in "Appendix" section. Equation (6) indicates that if the career is excited, then $|\frac{d\omega_t}{dt}| > 0$ and the planetary gear is backdriven because $\omega_t(0) = 0$.

Estimation of the excitation force

This section estimates the excitation force using the dynamic model. Let the vibration of amplitude e be given by $x = e\cos\omega_n t$, and F_{ex} be the excitation force. $|F_{\mathrm{ex}}|$ can be derived, as follows:

$$|F_{\mathrm{ex}}| = \frac{2\mu_{\mathrm{ax}}\tau_{\mathrm{rot}}}{mZ_4\cos\alpha}\left(1+\frac{Z_3}{Z_2}\right) + \widehat{M}\omega_n^2 e\cos\omega_n t, \tag{8}$$

where $\widehat{M} = M_1 + M_{23}$ denotes the total mass of the carrier, and μ_{ax} denotes the coefficient of friction in the axial direction. Equation (8) shows that $|F_{\mathrm{ex}}|$ increases as either τ_{rot} or ω_n increases. Detail of the derivation is described in "Appendix" section. Let us consider the appropriate vibrator for the device. Piezo elements can output sufficient excitation force for the proposed device but have difficulty in outputting sufficient amplitude compared with the backlash. To gain enough amplitude (≥ 0.3 mm), this study selects an eccentric cam for the vibrator. The required torque for the actuator τ_{cam} is calculated by

$$|\tau_{\mathrm{cam}}| = \frac{2\mu_{\mathrm{ax}}\tau_{\mathrm{rot}}}{mZ_4\cos\alpha}\left(1+\frac{Z_3}{Z_2}\right)e\sin\omega_n t + \widehat{M}\omega_n^2 e^2\sin\omega_n t\cos\omega_n t. \tag{9}$$

Herein, let us consider the estimation method of the required $|\tau_{\mathrm{cam}}|$. Because negative power consumption does not compensate for the positive power consumption[18], the simulation value of Eq. (9) is expected to be smaller than the experimental value in actuators. Moreover, because the purpose of estimation is to select the actuator, the estimated value would be slightly larger than the experimental value. Therefore, to estimate the approximately required $\widehat{\tau_{\mathrm{cam}}}$, this study uses the average $|\tau_{\mathrm{cam}}|$ during the acceleration phase ($0 \leq t \leq \frac{\pi}{2\omega_n}$). Assuming that $\mu_{\mathrm{ax}} \approx \mu$, then $|\widehat{\tau_{\mathrm{cam}}}|$ is calculated by

$$\widehat{\tau_{\mathrm{cam}}} = \frac{4\mu\tau_{\mathrm{rot}}}{\pi mZ_4\cos\alpha}\left(1+\frac{Z_3}{Z_2}\right)e + \frac{\widehat{M}}{\pi}\omega_n^2 e^2. \tag{10}$$

Simulation and experiments

Experimental setup

Figure 4(a) shows the developed planetary gear whose structure is illustrated in Fig. 4(b). Equation (4) indicates that the size of the device hardly affects the backdrivability. Thus, the size of the device is determined as shown in Fig. 4(a), for ease of assembly and disassembly. The range of $|\rho|$ is from 7.84 to 25.5, which is consistent with that of general planetary gear box. L and module m are set as 100 and 1 mm, respectively. Gears are fixed to the shaft via ETP bushes (Miki Pulley: ETP-A-15-B), for ease of assembling and disassembling. A DC motor (MABUCHI RS-735, reduction ratio: 8.5:1) is installed to drive the eccentric cam. Quenched stainless shafts (SUS440C) are used in the vibration part to prevent damage to the shafts. Moreover, the gears' surfaces are lubricated with molybdenum grease to prevent wearing.

The rest of this section is organized as follows: "Switching backdrivability of the developed device" section simply verifies whether backdrivability of the developed device can be switched; "Measurement of μ_s and μ_d" section experimentally estimates μ_s and μ_d for the backdrivability condition calculation of Eq. (4); "Backdrivability condition" section confirms the validity of the backdrivability condition calculation of Eq. (4); "Torque constant identification of the vibrator" section identifies the torque constant of the vibrator and "Required vibrator torque" section estimates the excitation force from the vibrator current to verify the validity of Eq. (10) (i.e., whether $|F_{\mathrm{ex}}|$ increases as either τ_{rot} or ω_n increases).

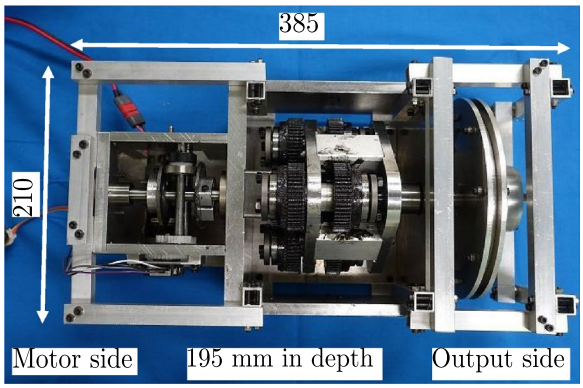

(a) Developed device.

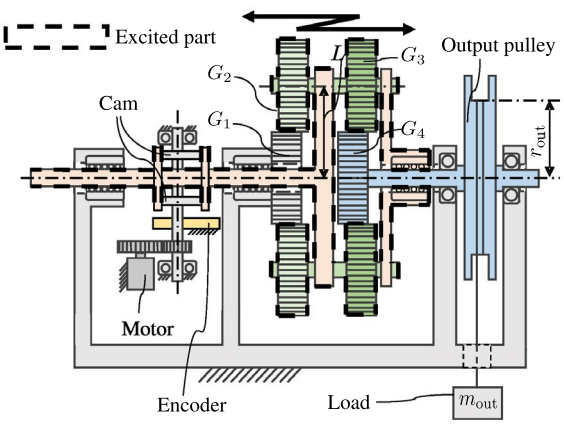

(b) Schematic diagram.

Fig. 4 Developed planetary gear

Switching backdrivability of the developed device

To verify whether backdrivability of the developed device can be switched, the input shaft is excited. Figure 5 shows the experimental results for switching backdrivability where $m_{out} = 1.0$ kg, $r_{out} = 75$ mm and $(Z_1, Z_4) = (50, 49)$. The load remained motionless between 0 to 14.5 s of the no-vibration state and, fell down after 14.5 s of the vibration state. These results indicate that vibration can switch the backdrivability of the proposed device.

Measurement of μ_s and μ_d

To calculate backdrivability condition of Eq. (4), μ_s and μ_d are experimentally estimated. Because $\eta_{ij} \geq 0.9$, estimation of η_{ij} from a pair of gears requires accurate force measurement, causing difficulty in estimating μ_s and μ_d. Therefore, this study estimates μ from total efficiency η_{gross} of the device in the forward drive. η_{gross} is calculated by Ryokaku's method[13] as follows:

$$\eta_{gross} = \begin{cases} \dfrac{1-\frac{z_1}{z_2}\frac{z_2}{z_4}}{1-\eta_{12}\eta_{34}\frac{z_1}{z_2}\frac{z_3}{z_4}}, & (z_1 < z_4) \\ \dfrac{1-\frac{z_1}{z_2}\frac{z_3}{z_4}}{1-\frac{1}{\eta_{12}\eta_{34}\frac{z_1}{z_2}\frac{z_3}{z_4}}}, & (z_1 > z_4) \end{cases} \tag{11}$$

Assuming $\mu^2 \approx 0$ and $\mu\frac{n}{Z_i} \approx 0$, then Eqs. (19) and (11) can derive μ as follows:

$$\mu \approx \frac{\left(\frac{1}{\eta_{gross}} - 1\right)\left|\frac{Z_2 Z_4}{Z_1 Z_3} - 1\right|}{\pi h_{12}\left(\frac{1}{Z_1} + \frac{1}{Z_2}\right) + \pi h_{34}\left(\frac{1}{Z_3} + \frac{1}{Z_4}\right)}, \tag{12}$$

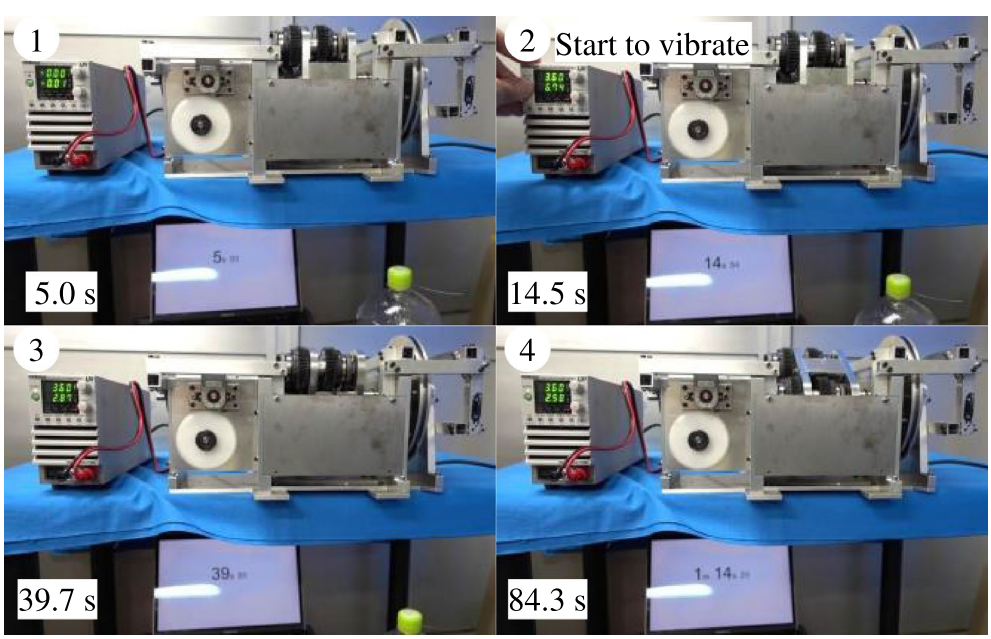

Fig. 5 Experimental results of switching backdrivability of developed device. The input voltage for the vibrator was set as 3.6 V

where h_{ij} is defined by

$$h_{ij} = \left(1 - \varepsilon_i - \varepsilon_j + \varepsilon_i^2 + \varepsilon_j^2\right). \tag{13}$$

Figure 6(a) shows the experimental setup for μ_s measurement. To measure η_{gross} at the beginning of the forward drive, we gradually increase the load of the input shaft while applying a constant load (29.4 N) to the output pulley. η_{gross} is calculated by

$$\eta_{\text{gross}} = \frac{m_{\text{out}} g r_{\text{out}}}{m_{\text{in}} g r_{\text{in}}}. \tag{14}$$

In the experiments, η_{gross} was 0.423, which resulted in $\mu_s = 0.271$ where $m_{\text{out}} = 3.0$ kg, $(r_{\text{in}}, r_{\text{out}}) = (100, 75)$ mm and $(Z_1, Z_4) = (50, 49)$.

Figure 6(b) shows the experimental setup for μ_d estimation. A motor pulls a wire; the tensile force of the wire is measured by a force gauge (AIKOH, RZ-10). η_{gross} was 0.533, which resulted in $\mu_d = 0.174$; the other conditions were the same as those of μ_s measurement experiments.

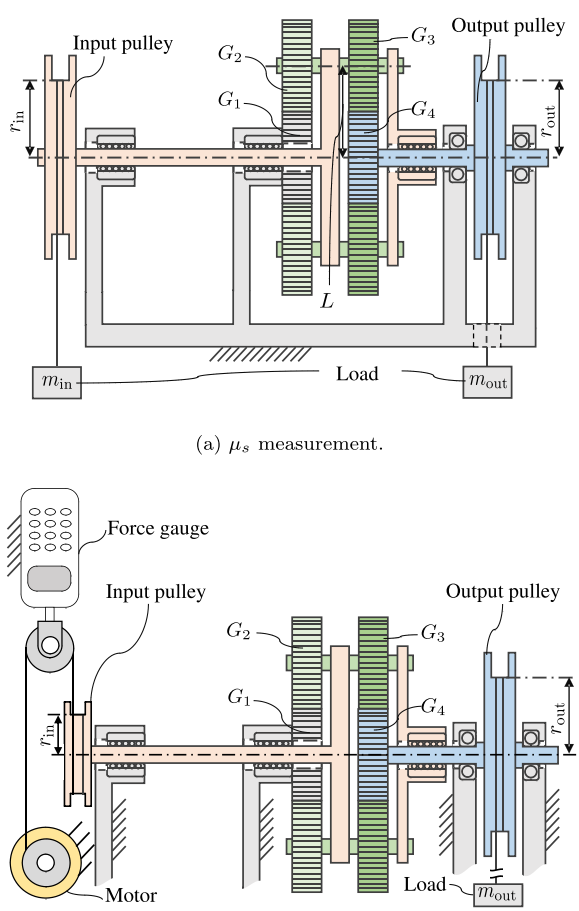

(a) μ_s measurement.

(b) μ_d measurement.

Fig. 6 Experimental setup for μ measurement

Backdrivability condition

We performed backdrivability experiments to verify the backdrivability conditions of Eq. (4). Within $1 \leq n \leq 3$, Z_1 and Z_4 are set as shown in Table 1. To approximate $|\xi|$ to $\overline{p_{ij}}$, Z_1 and Z_4 are set as $3i \pm 1$ $(i = 1, 2 \ldots)$. A load is applied to the output pulley at static conditions, and the carrier rotation is confirmed. The load is adjusted so that the maximum τ_{rot} becomes 3.68 N · m.

Table 1 summarizes the experimental results of the backdrivability. The reducer was less likely to be back driven when $n = 1$, while it was back driven when $n \geq 2$. In simulation, $\mu_s \Lambda < 1$ when $n \geq 2$ and $\mu_s = 0.271$. Thus, the experimental results are consistent with the simulation result of Eq. (4).

Note: The maximum τ_{rot} is determined depending on tooth face and bending strength.

Torque constant identification of the vibrator

To estimate the torque from the speed and current of the vibrator, torque constant identification of the vibrator is performed. An arm, in contact with a force gauge (AIKOH, RZ-20), is attached to the rotational axis of the vibration part. A DC stabilization power unit (Kikusui: PWR401L) changes the input voltage V_{in} and measures the current. This study calculates $|\overline{\tau_{\text{cam}}}|$ from the input current i_{in}, as follows:

$$|\overline{\tau_{\text{cam}}}| = C_1 i_{\text{in}} + C_2. \tag{15}$$

The vibrator contains viscous resistance $|\overline{\tau_{\text{loss}}}|$ [19, 20], identified by the following equation

$$|\overline{\tau_{\text{loss}}}| = C_3 \omega_n + C_4. \tag{16}$$

To derive Eq. (16), we confirm the relationship between $|\overline{i_{\text{loss}}}|$ and ω_n where no load is applied to the vibrator. A DC stabilization power unit (Kikusui: PWR401L) changes V_{in} (1.0–1.9 V), and measures i_{loss}. Referring to [20], the following approximate expression was used:

$$|\overline{i_{\text{loss}}}| = C_5 \omega_n + C_6. \tag{17}$$

Fig. 7(a) shows the current-torque relationship, and Fig. 7(b) shows the current-angular-velocity relationship. These results identifies C_1–C_6 as summarized in Table 2.

Note 1: This identification is significant because individual difference and assembling cause torque constant variation.

Note 2: Because the vibrator did not rotate when $V_{\text{in}} < 1.0$ V, V_{in} was set as ≥ 1.0 V.

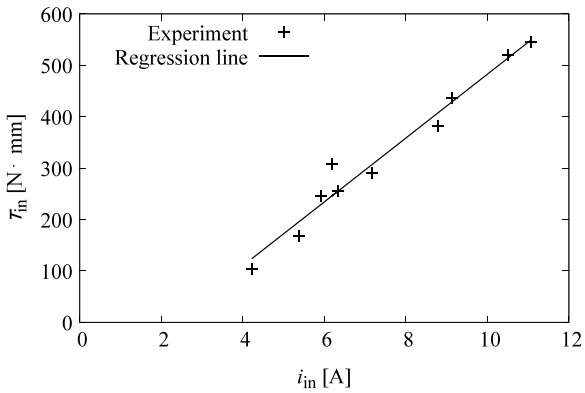

(a) Torque effects.

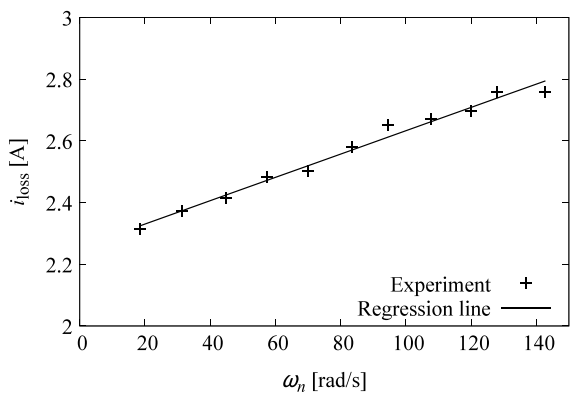

(b) Viscosity effects.

Fig. 7 Calibration results of the motor specification

Required vibrator torque

To verify the validity of Eq. (10), the excitation force of the vibrator is measured. To estimate the excitation force, we measure the vibrator current. Figure 4(b) shows the experimental setup of the vibrating planetary gear carrier. Z_1 and Z_4 are set as 49 and 50, respectively, and e is designed as 1 mm. $\widehat{M}$ became 3.82 kg, and $\widehat{I}$, calculated by CAD Software (SolidWorks 2021), is 2.79 kgm^2. A DC stabilization power unit (Kikusui: PWR401L) changes the value of V_{in}, and an encoder (CUI-DEVICE: AMT102-V) measures the value of ω_n. V_{in} is set as 3.6, 6.2, and 8.8 V so that the approximate frequency of the vibration will become 5, 10, and 15 Hz respectively. i_{in} is measured by a current sensor(Pololu: ACS714), whose signal is converted by an analog-digital-converter (Elmos: RAI-16, sampling rate: 10 kHz). τ_{rot} varies from 0.368 to 3.68 N · mm, and each load test is performed five times.

Figure 8 shows the measurement results of required current and angular velocity, and Fig. 9 shows the estimated result of $|\overline{\tau_{cam}}|$. i_{in} is the average value during 0.5 s of the beginning phase of the eccentric-cam's constant rotation. i_{in} data at $\tau_{rot} = 0.368$ N · mm, and $V_{in} = 3.6, 6.2$ V does not exist because the output shaft was not back driven. Figure 9 also illustrates the simulation result of $|\widehat{\tau_{cam}}|$. $|\widehat{\tau_{cam}}|$ is simulated at an average angular velocity $\overline{\omega_n}$. The graphs of Fig. 9 indicate that $|\overline{\tau_{cam}}|$ increases with increasing τ_{rot} and ω_n. Though the required torque is smaller than that simulated at $V_{in} = 3.6$ V, the experimental results of the required torque are mostly consistent with the simulation results of Eq. (10). Note: The beginning phase of the eccentric-cam's constant rotation phase was determined by the time history of the current and angular velocity.

Discussion

Certainty of non-backdrivability

In the backdrivability condition experiments, the developed device became less-backdrivable when the tooth number difference was 1. Thus, the value of $\mu\Lambda$ are consistent with the backdrivability condition of Eq. (4). In practical condition, the value of μ depends on temperature, humidity and wearing of the gear surfaces[21]. Furthermore, because Λ is estimated in the average efficiency engagement, the value of Λ will fluctuate with real engagement situations. Although μ and Λ varies, the experimental results indicate that the proposed method can approximately judge the less-likely-backdrivability of the 2K-H planetary gear.

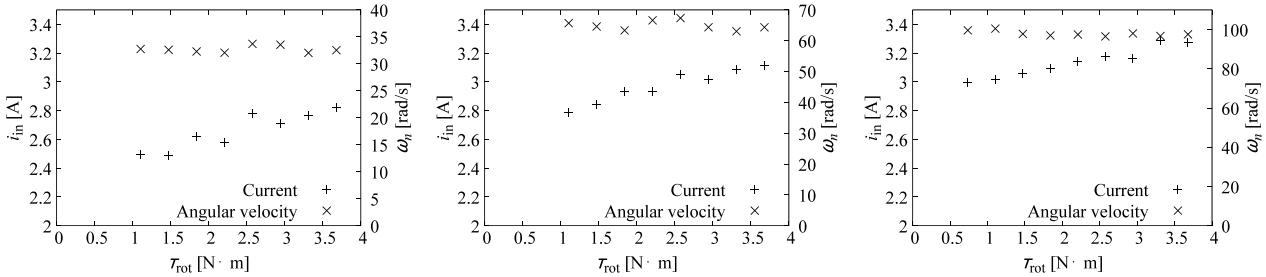

(a) $V_{in} = 3.6$ V ($\overline{\omega_n} = 32.9$ rad/s). (b) $V_{in} = 6.2$ V ($\overline{\omega_n} = 64.9$ rad/s). (c) $V_{in} = 8.8$ V ($\overline{\omega_n} = 98.3$ rad/s).

Fig. 8 Experimental results of the required current

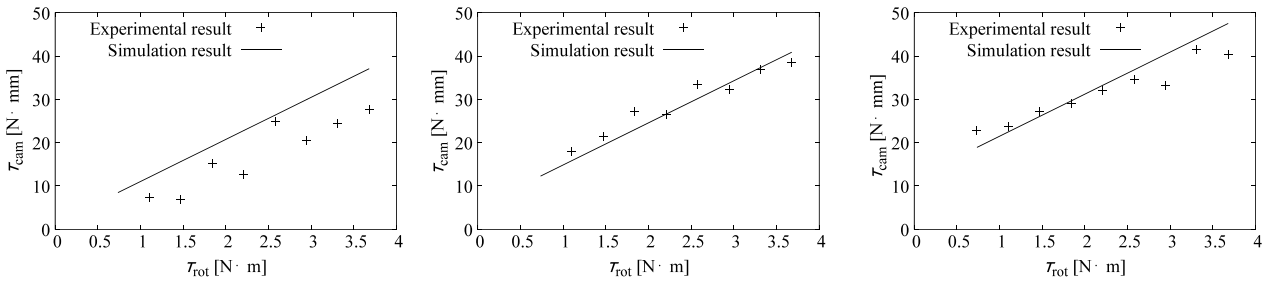

(a) $V_{in} = 3.6$ V ($\overline{\omega_n} = 32.9$ rad/s). (b) $V_{in} = 6.2$ V ($\overline{\omega_n} = 64.9$ rad/s). (c) $V_{in} = 8.8$ V ($\overline{\omega_n} = 98.3$ rad/s).

Fig. 9 Calculated results of the required torque

Estimation of the excitation force

The experimental results show that $\overline{\tau_{cam}}$ increases as τ_{rot} and ω_n increase. Although the required torque became smaller than estimated $V_{in} = 3.6$ V, the experimental and simulation results are mostly consistent. Because the decrease of estimated value at $V_{in} = 3.6$ V was small, the proposed method can estimate the required torque for switching backdrivability of 2K-H planetary gear.

The decrease can be attributed to a discrepancy between μ_{ax} and μ. Because μ_{ax} decreases as $\overline{\omega_n}$ decreases, μ_{ax} became much smaller than μ, resulting in $\overline{\tau_{cam}}$ decrease.

The cause of the non-backdriven output shaft at $\tau_{rot} = 0.368$ N · mm, and $V = 3.6, 6.2$ V can be attributed to the friction at the linear bush. The coefficient of friction at linear bush will be similar to Eq. (39) as described in "Appendix" section. Therefore, the switching backdrivability will likely occur as ω_n increases.

Output shaft motion after quitting vibration

In the experiments, the backdrive motion continued after quitting the vibration. Because μ becomes μ_d after quitting the vibration, Eq. (6) can derive $I\frac{d\omega_t}{dt} > (1 - \mu_d\Lambda)\tau_{rot}$. Thus, these results are consistent with the estimation of Eq. (6).

$\mu_d\Lambda$ is expected to be > 1 to stop the backdrive motion after quitting the vibration. Referring to [17], the use of profile-shifted gears is effective to increase $\mu_d\Lambda$.

Miniaturization of the vibrator

This study assumes that the backdrive motion is only performed in emergency cases and is not frequently used. Hence, this study does not focus on reducing the energy consumption of the vibrator. If reducing the expected energy is expected, using a resonance will be effective.

Conclusion

To systematically design switching backdrivable 2K-H planetary gear, this study reveals less back-drive condition and the required torque for a vibrator. We then discuss the less-backdrivable condition and required force for the vibrator. Based on the simulation and experiments, we confirm the following:

- In the less-backdrivable condition, the tooth number difference between the fixed and output gears are dominant. It was less-backdrivable when the tooth number difference was 1.
- The required torque for the vibrator increases as the output shaft load and vibration frequency increases. The experimental results are almost entirely consistent with simulation result of dynamic model.

These results indicate that the dynamic model of 2K-H planetary gear can predict the switching backdrivability phenomenon. Profile shifted gears to stop the backdrive motion after quitting the vibration will be considered in our future work.

Appendix

Derivation of Eq. (4)

We consider the mesh efficiency of the gear pair to discuss the less-likely-backdrive condition of the proposed planetary gear. Let ξ denote the distance from the pitch point. Referring to [12], the efficiency between G_i and G_j at ξ is given by

$$\eta_{ij} = 1 - \frac{2\mu_{ij}|\xi|}{m_{ij}\cos\alpha}\left(\frac{1}{Z_i} + \frac{1}{Z_j}\right). \tag{18}$$

ξ depends on the rotational angle of G_i, causing difficulty in discussing the backdrivability of the proposed planetary gear.

Herein, let us consider the expected value of ξ. This study focuses on Niemann's equations given by

$$\eta_{ij} = 1 - \mu_{ij}\pi\left(1 - \varepsilon_i - \varepsilon_j + \varepsilon_i^2 + \varepsilon_j^2\right)\left(\frac{1}{Z_i} + \frac{1}{Z_j}\right). \tag{19}$$

Comparing (18) and (19), this study defines expected value $\overline{p_{ij}}$ of $|\xi|$ as follows:

$$\overline{p_{ij}} = \frac{1}{2} m_{ij}\pi \left(1 - \varepsilon_i - \varepsilon_j + \varepsilon_i^2 + \varepsilon_j^2\right) \cos\alpha. \tag{20}$$

$F_{ijt} = \mu_{ij} F_{ijn}$ when gears begin to backdrive; thus, the translation motion equation of G_2 and G_3 is given by

$$-M_{23}(R_1 + R_2)\rho \frac{d\omega_t}{dt} = b_{\text{sign}} F_{\text{rot}} + F_{12n} A_{12} - F_{34n} A_{34}, \tag{21}$$

A_{12} and A_{34} denote

$$A_{12} = \cos\alpha \pm \mu_{12} \sin\alpha \tag{22}$$

$$A_{34} = \cos\alpha \pm \mu_{34} \sin\alpha, \tag{23}$$

where double signs are in random order. A rotational motion equation of G_2 and G_3 at the center of mass is given by

$$\begin{aligned} I_{23}\left(1 + \frac{Z_1}{Z_2}\right)\rho \frac{d\omega_t}{dt} &= F_{12n} R_2 A_{12} - F_{34n} R_3 A_{34} \\ &- b_{\text{sign}}(\mu_{12}\overline{p_{12}} F_{12n} + \mu_{34}\overline{p_{34}} F_{34n}) \end{aligned} \tag{24}$$

The motion equation of the output shaft is given by

$$I_4 \frac{d\omega_t}{dt} = -F_{34n}(A_{34} R_4 + \mu_{34}\overline{p_{34}}) + \tau_{\text{rot}}. \tag{25}$$

Because the planetary gear is static in this state, static analysis is significant. If $\frac{d\omega_t}{dt} = 0$, then F_{34n}, F_{rot} and $F_{12\text{n}}$ are derived as follows:

$$F_{34n} = \frac{1}{A_{34} R_4 + \mu_{34}\overline{p_{34}}} \tau_{\text{rot}} \tag{26}$$

$$F_{12n} = F_{34n} \frac{A_{34} R_3 + b_{\text{sign}} \mu_{34} |\overline{p_{34}}|}{A_{12} R_2 - b_{\text{sign}} \mu_{12} |\overline{p_{12}}|} \tag{27}$$

$$\begin{aligned} F_{\text{rot}} = & F_{34n} \frac{A_{12} A_{34}}{A_{12} R_2 - b_{\text{sign}} \mu_{12} |\overline{p_{12}}|} \\ & \times \left(|\ell| - \mu_{12} \frac{|\overline{p_{12}}|}{A_{12}} - \mu_{34} \frac{|\overline{p_{34}}|}{A_{34}}\right). \end{aligned} \tag{28}$$

If the planetary gear is backdrived without vibration, F_{rot} must satisfy

$$F_{\text{rot}} \geq 0, \tag{29}$$

thus

$$|\ell| - \left(\mu_{12} \frac{|\overline{p_{12}}|}{A_{12}} + \mu_{34} \frac{|\overline{p_{34}}|}{A_{34}}\right) \geq 0. \tag{30}$$

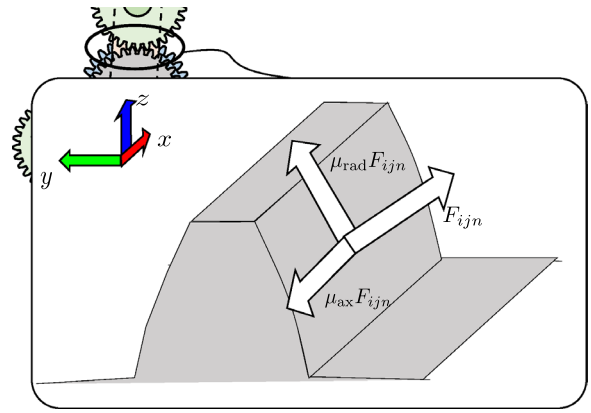

Fig. 10 Force acting on the gears when the carrier is excited

Table 1 Experimental result of backdrivability

n	Z_1	Z_4	ρ	$\mu_s \Lambda$	Existence of non-backdriven point
1	49	50	25.5	1.34	Yes
	50	49	−24.5	1.34	Yes
2	50	52	13	0.668	No
	52	50	-12	0.668	No
3	49	52	8.84	0.445	No
	52	49	−7.84	0.445	No

Table 2 Calibration result of C_1 to C_6

Item		Value
C_1	[N · mm/A]	62.1
C_2	[N · mm]	−138
C_3	[N · mm s / rad]	0.235
C_4	[N · mm]	1.69
C_5	[A s/ rad]	0.00378
C_6	[A]	2.25

Let m be $m = m_{12} = m_{34}$. Assuming $\mu \ll 1$, $\mu^2 \approx 0$ and $\frac{\mu}{Z_i} \approx 0$, then Eq. (30) become

$$\mu\Lambda \leq 1. \tag{31}$$

Alternatively, the proposed mechanism is less likely to backdrive when $\mu\Lambda > 1$.

Preparation for derivation of Eqs. (6) and (8)

To derive Eqs. (6) and (8), this section discusses μ_{rad} and μ_{ax}, the coefficient of friction in the radial and axial direction, respectively. Figure 10 illustrates the force acting on the gear surface when the carrier is excited. Because

friction force acts in the x direction, total friction force μF_{ijn} becomes:

$$\mu F_{ijn} = \sqrt{\mu_{\mathrm{ax}}^2 + \mu_{\mathrm{rad}}^2} F_{ijn}. \tag{32}$$

The dynamic friction force is assumed to act in the relative velocity direction of the tooth surface. v_{rel}, which denotes the relative velocity in the tangential direction between G_i and G_j, is calculated by

$$|v_{\mathrm{rel}}| = \left(1 + \frac{Z_j}{Z_i}\right)|\xi|\omega_i, \tag{33}$$

where ω_i denotes the angular velocity of G_i.

Let v_{rad} and v_{ax} be the relative velocity of the radial and axial direction of the tooth surface, respectively. Thus, the relative velocity $\overline{v_{\mathrm{rad}}^{p12}}$ in the tangential direction between G_1 and G_2 and $\overline{v_{\mathrm{rad}}^{p34}}$ is calculated by

$$\overline{v_{\mathrm{rad}}^{p12}} = \overline{p_{12}}\left(1 + \frac{Z_2}{Z_1}\right)\frac{Z_4}{Z_3}|(\rho - 1)\omega_t| \tag{34}$$

$$\overline{v_{\mathrm{rad}}^{p34}} = \overline{p_{34}}\left(1 + \frac{Z_4}{Z_3}\right)|(\rho - 1)\omega_t|. \tag{35}$$

Let us consider the numerical value of $\overline{p_{ij}}$. Because $h_{12} \approx h_{34} \approx \frac{n\Lambda}{2\pi}$ (see "Mechanical analysis for backdrivability" section and Fig. 3), this study assumes $\overline{p_{12}} \approx \overline{p_{34})} \approx \overline{p}$; $\overline{p}$ is defined by

$$\overline{p} = \frac{\overline{p_{12}} + \overline{p_{34}}}{2}. \tag{36}$$

This study also assumes $\overline{v_{\mathrm{rad}}^{p12}} \approx \overline{v_{\mathrm{rad}}^{p34}}$, and $\overline{v_{\mathrm{rad}}}$ is defined by

$$\begin{aligned}\overline{v_{\mathrm{rad}}} =& \frac{\overline{v_{\mathrm{rad}}^{p12}} + \overline{v_{\mathrm{rad}}^{p34}}}{2} \\ =& \overline{p}\left(\frac{Z_4}{Z_3} + \frac{Z_2 Z_4}{2Z_1 Z_3} + \frac{1}{2}\right)|(\rho - 1)\omega_t|.\end{aligned} \tag{37}$$

Let ω_n be the angular velocity of vibrator. Because the period of the vibrator T is given by $T = \frac{2\pi}{\omega_n}$, $\overline{v_{\mathrm{ax}}}$ is given as follows:

$$\overline{v_{\mathrm{ax}}} = \frac{4e}{T} = \frac{2e}{\pi}\omega_n. \tag{38}$$

Hence, μ_{rad} and μ_{ax} are denoted by

$$\mu_{\mathrm{rad}} = \mu\frac{|\overline{v_{\mathrm{rad}}}|}{\sqrt{\overline{v_{\mathrm{ax}}}^2 + \overline{v_{\mathrm{rad}}}^2}} = \mu\frac{|\omega_t|}{\sqrt{\omega_t^2 + \lambda^2\omega_n^2}} \tag{39}$$

$$\mu_{\mathrm{ax}} = \mu\frac{|\overline{v_{\mathrm{ax}}}|}{\sqrt{\overline{v_{\mathrm{ax}}}^2 + \overline{v_{\mathrm{rad}}}^2}} = \mu\frac{\lambda|\omega_n|}{\sqrt{\omega_t^2 + \lambda^2\omega_n^2}}, \tag{40}$$

where λ is defined by

$$\lambda = \frac{\overline{v_{\mathrm{ax}}}|\omega_t|}{\overline{v_{\mathrm{rad}}}|\omega_n|} = \frac{e}{\pi\overline{p}}\frac{1}{|\rho - 1|}\frac{4Z_1 Z_3}{(Z_1 + Z_2)(Z_1 + Z_4)}. \tag{41}$$

Derivation of Eqs. (6) and (8)

This section derive Eqs. (6) and (8) from motion equations. The dynamic equation of G_1 is given by

$$I_1\rho\frac{d\omega_t}{dt} = b_{\mathrm{sign}}F_{\mathrm{rot}}(R_1 + R_2). \tag{42}$$

Assuming $\mu\frac{I_4}{\widehat{I}} \approx 0$, $\mu\frac{1}{Z_i} \approx 0$ and $\mu = \mu_d$, then Eqs. (21), (24), (25) and (42) can derive

$$\widehat{I}\frac{d\omega_t}{dt} + \tau_{\mathrm{rot}}\frac{\mu_d\Lambda|\omega_t|}{\sqrt{\omega_t^2 + \lambda^2\omega_n^2}} = \tau_{\mathrm{rot}}. \tag{6}$$

Let x be the displacement of the carrier in axial direction, and the dynamic motion equation is given by

$$\widehat{M}\frac{d^2x}{dt^2} = F_{\mathrm{ex}} - \mathrm{sgn}(\dot{x})\mu_{\mathrm{ax}}(F_{12n} + F_{34n}). \tag{43}$$

Assuming $\mu\frac{I_4}{\widehat{I}} \approx 0$, $\mu\frac{1}{Z_i} \approx 0$ and $\mu = \mu_d$, then Eqs. (21), (24), (25) and (43) can derive

$$|F_{\mathrm{ex}}| = \frac{2\mu_{\mathrm{ax}}\tau_{\mathrm{rot}}}{mZ_4\cos\alpha}\left(1 + \frac{Z_3}{Z_2}\right) + \widehat{M}\omega_n^2 e\cos\omega_n t. \tag{8}$$

Acknowledgements
We acknowledge Yuji Fujita and Shogo Yoshida for designing the experimental device prototype. We would like to thank Editage (www.editage.com) for English language editing.

Author contributions
SN and KY invented the proposed mechanisms. SN, RI and KE conducted the examinations. TT refined the proposed mechanism and improved the quality of principles. All authors read and approved the final manuscript.

Funding
This work was supported by JSPS KAKENHI Grant Number JP20K14704.

Availability of data and materials
The datasets supporting the conclusions of this article are included within the article.

Declarations

Ethics approval and consent to participate
Not applicable.

Consent for publication
Not applicable.

Competing interests
The authors declare that they have no competing interests.

Received: 14 May 2023 Accepted: 19 October 2023
Published online: 10 November 2023

References

1. Takeichi M, Suzumori K, Endo G, Nabae H (2017) Development of giacometti arm with balloon body. IEEE Robot Automation Lett 2(2):951–957
2. Renda F, Giorelli M, Calisti M, Cianchetti M, Laschi C (2014) Dynamic model of a multibending soft robot arm driven by cables. IEEE Trans Robotics 30(5):1109–1122
3. Al-Ibadi A, Nefti-Meziani S, Davis S, Theodoridis T (2018) Novel design and position control strategy of a soft robot arm. Robotics 7(4):72
4. Matsuno T, Wang Z, Hirai S (2017) Grasping state estimation of printable soft gripper using electro-conductive yarn. Robot Biomimet 4(1):1–11
5. Suyama A, Aiyama Y (2018) Development of new teaching method for industrial robot using visual information. Trans Japan Soc Mechan Eng 84(865):18–00153)
6. Oiwa T, Makino Y, Satou M, Asama J (2011) Friction reduction and lubricity improvement for meshed gears based on ultrasonic oscillation (design and trial construction of gear shaft). Trans Japan Soc Mechan Eng Series C 77(775):737–74
7. Matsui N, Shirafuji S, Ota J (2016) Locking mechanism based on flat, overlapping belt, and ultrasonic vibration. IEEE Inter Conf Robot Biomim (ROBIO) 1:461–466
8. Kumar V, Hutchings I (2004) Reduction of the sliding friction of metals by the application of longitudinal or transverse ultrasonic vibration. Tribol Int 37(10):833–840
9. Takayama T, Hisamatsu N (2019) Worm gear mechanism with switchable backdrivability. ROBOMECH J 6(1):1–10
10. Hisamatsu N, Takayama T, Omata T (2013) Worm gear that can change its backdrivability. In: Proceedings of the 2013 JSME Conference on Robotics and Mechatronics, pp. 2–1031. The Japan Society of Mechanical Engineers.
11. Takayama T, Hisamatsu N, Omata T (2014) Worm gear with switchable backdrivability–2nd report, the influence that vibration direction gives in backdrivability–. In: Proceedings of the 2014 JSME Conference on Robotics and Mechatronics, pp. 2–2051. The Japan Society of Mechanical Engineers.
12. Yada T (1997) Review of gear efficiency equation and force treatment. JSME Int J Ser Dynamics Control Robot Design Manuf 40(1):1–8
13. Morozumi M, Kishi S (1983) Torque distribution in planetary gears (1st report, 2k-h type planetary gear). J Faculty Eng Shinshu UniV 54:1–14
14. Jianying L, Qingchun H, Changfu Z, Tianjun Z (2017) Power analysis and efficiency calculation of multistage micro-planetary transmission. Energy Procedia 141:654–659
15. Yamanobe K, Noda S, Takayama T (2019) Study on planetary gear with switchable backdrivability-1st report, the confirmation of the non-backdrivable condition and the basic movement-. In: Proceedings of the 2019 JSME Conference on Robotics and Mechatronics, pp. 1–103. The Japan Society of Mechanical Engineers
16. Fujita Y, Noda S, Takayama T (2020) Study on planetary gear with switchable backdrivability-2nd report, suitable parameter for the switching and backdrive behavior observation-. In: Proceedings of the 2020 JSME Conference on Robotics and Mechatronics, pp. 1–101. The Japan Society of Mechanical Engineers
17. Matsuki H, Nagano K, Fujimoto Y (2019) Bilateral drive gear-a highly backdrivable reduction gearbox for robotic actuators. IEEE/ASME Trans Mechatron 24(6):2661–2673
18. Hirose S, Fukuda Y, Yoneda K, Nagakubo A, Tsukagoshi H, Arikawa K, Endo G, Doi T, Hodoshima R (2009) Quadruped walking robots at tokyo institute of technology. IEEE Robot Automation Magazine 16(2):104–114
19. Hirose S (2008) Robotics -vector analysis of mechanical system. Shokabo, Tokyo
20. Endo D, Nagatani K, Yoshida K (2015) Study on how to sense slippage by motor-tractve-currents for odometry of tracked vehicle. J Robot Soc Japan 33(6):433–440
21. Oiwa T, Makino Y, Asama J (2012) Friction reduction and lubricity improvement for meshed gears based on ultrasonic oscillation (experiment of friction reduction on the tooth frank). Trans Japan Soc Mechan Eng Series C 78(788):1242–1249

Publisher's Note